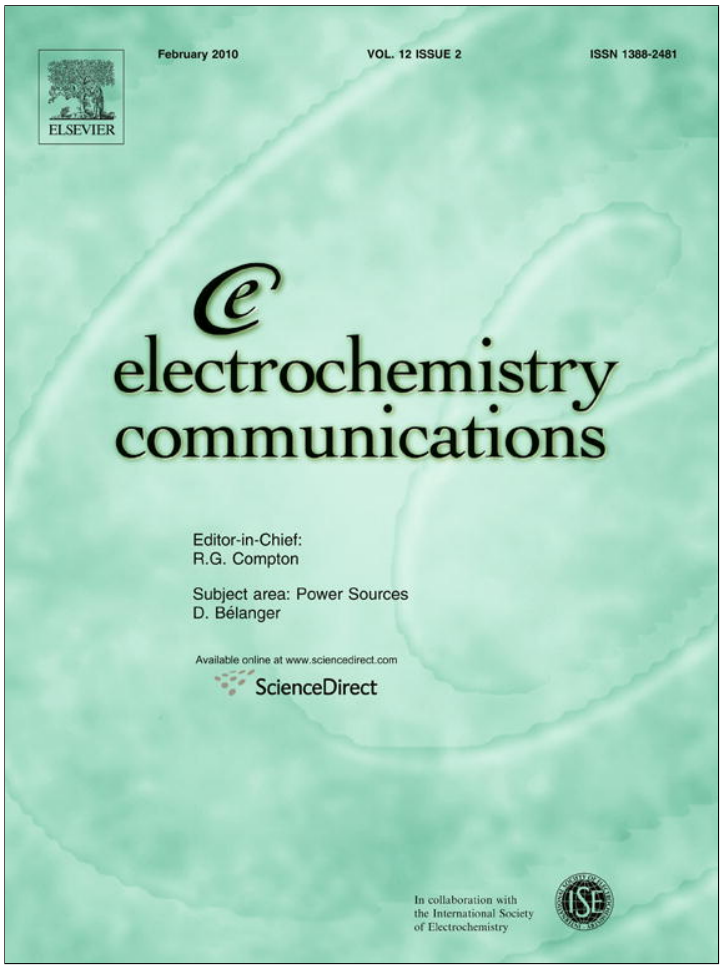

Electrochemistry Communications 12 (2010) 223–226

Contents lists available at ScienceDirect

Electrochemistry Communications

journal homepage: www.elsevier.com/locate/elecom

Kinetic Monte Carlo simulations of oxygen vacancy diffusion in a solid electrolyte: Computing the electrical impedance using the fluctuation–dissipation theorem

Eunseok Lee *, Friedrich B. Prinz, Wei Cai

Department of Mechanical Engineering, Stanford University, Stanford, CA 94305, USA

ARTICLE INFO

Article history:
Received 12 September 2009
Received in revised form 3 November 2009
Accepted 29 November 2009
Available online 5 December 2009

Keywords:
Kinetic Monte Carlo simulation
Fluctuation–dissipation theorem
Electrochemical impedance spectroscopy
Solid electrolyte
Ionic conductivity

ABSTRACT

We present a new method for computing the electrical impedance of solid oxide electrolyte from kinetic Monte Carlo simulations of oxygen vacancy diffusion. The impedance values at all frequencies are obtained from a single equilibrium simulation based on the fluctuation–dissipation theorem, leading to a significant gain of efficiency over existing methods.This allows us to systematically examine the effect of dopant concentration. Increasing dopant concentration is found to decrease the infinite-frequency impedance, which is attributed to the increasing density of oxygen vacancies. The difference between the impedance values at zero- and infinite-frequency, on the other hand, shows the opposite trend, and is linked to dopant–vacancy interactions. Hence the two competing mechanisms, previously proposed to explain the existence of an optimal doping concentration, are separately quantified.Our model also predicts a significant effect of the arrangement of dopant cations on the electrolyte conductivity.

1. Introduction

Improving the ionic conductivity of solid electrolytes is an important step in reducing the operating temperature of solid oxide fuel cells (SOFCs), which is a goal that drives extensive contemporary research worldwide [1,2]. In order to engineer better electrolyte materials, it is desirable to separately quantify the various mechanisms that contribute to ionic conductivity. For example, in electrochemical impedance spectroscopy (EIS), the grain, grain boundary and electrode contributions to total conductivity can be separately identified from different signatures in the Nyquist plot of the impedance function [3].

The impedance function can also be computed from simulations based on fundamental mechanisms of charge diffusion [4–7]. The simulation predictions are useful in reducing the uncertainties in the interpretations of the measured impedance spectra.The existing computational method closely mimics the experimental procedure. An AC voltage is applied to the simulation cell and the response AC current is obtained from the ensemble average of the charge velocities.The main drawback of this approach is the excessive computational cost; at least one independent simulation is required to compute the impedance at each frequency of interest.Furthermore, if the frequency is low, it takes a long time to simulate even one AC period, whereas averaging over many AC periods is needed to remove statistical noise.

In this paper, we show that the impedance at all frequencies can be computed from a single equilibrium simulation, by using the fluctuation–dissipation theorem (FDT). This leads to a substantial increase of computational efficiency from the existing methods. The new method allows us to systematically examine the effect of dopant concentration on the bulk impedance function.It provides quantitative measures to the two competing mechanisms previously proposed to explain the existence of an maximum conductivity as a function of doping concentration.Our simulations also predicts that engineering the spatial distribution of dopant cations has the potential to significantly improve the electrolyte conductivity.

2. Kinetic Monte Carlo model

We focus on the kinetic Monte Carlo (kMC) model of oxygen vacancy diffusion in cubic yttria–stablized-zirconia (YSZ), a widely used solid electrolyte [8]. Because the oxygen anions form a simple-cubic sub-lattice, every oxygen vacancy can move to six nearest-neighbor positions $(\pm x, \pm y, \pm z)$ in each kMC step. The total number of possible jumps in each step is $6N$ where N is the number of vacancies. The rate for each vacancy jump k is $j_k = v_0 \exp\left[-\frac{\Delta G_k}{k_B T}\right]$, where v_0 is a trial frequency[1] and ΔG_k is the activation barrier. ΔG_k

* Corresponding author. Tel.: +1 6507761557; fax: +1 6507231778.
E-mail address: euniv@stanford.edu (E. Lee).

[1] For simplicity, we choose $v_0 = 10^{13}\ s^{-1}$ in this work, following [6] and [7]. Changing v_0 will only rescale the frequency axis of the impedance function $Z(\omega)$ and will not change the Nyquist plot and the main conclusion of this paper.

1388-2481/$ - see front matter © 2009 Elsevier B.V. All rights reserved.
doi:10.1016/j.elecom.2009.11.031

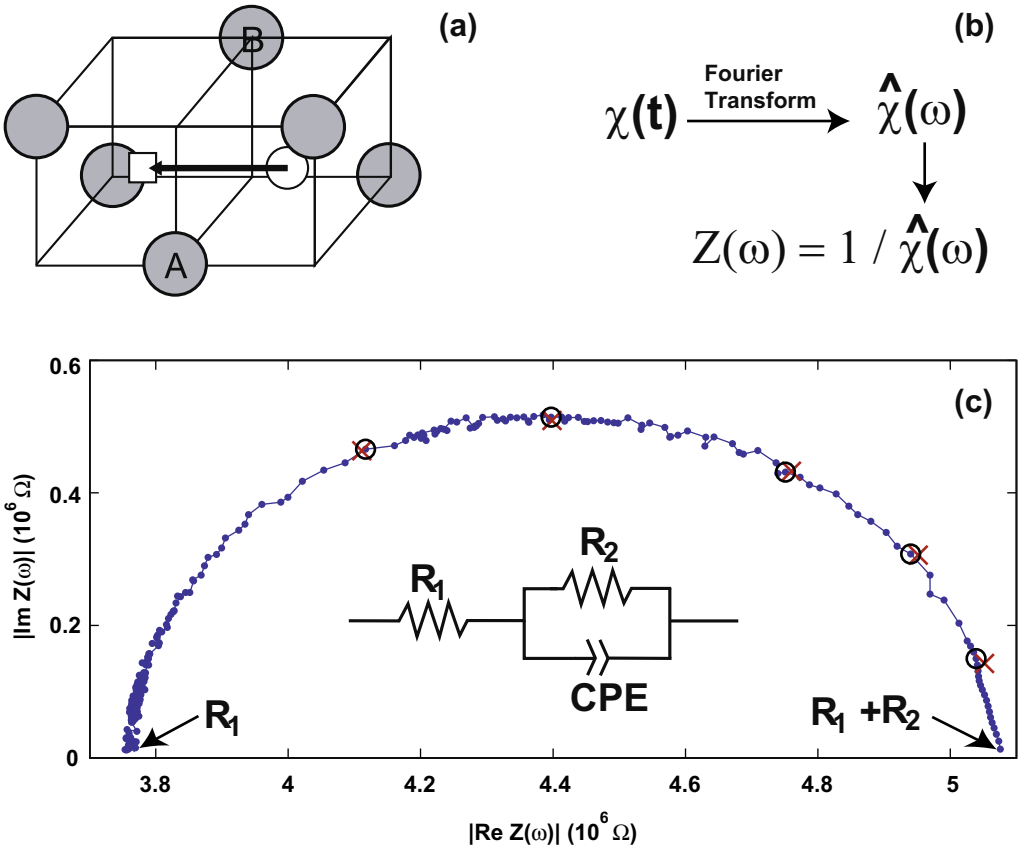

Fig. 1. (a) A vacancy migration cell in YSZ. Gray circles are cations (Zr or Y), the white circle is an oxygen anion, and the white square is the oxygen vacancy. The energy barrier for vacancy migration is assumed to depend only on the chemical species of cations A and B [6]. $\Delta G_k = 0.58$ eV when both cations are Zr, $\Delta G_k = 1.27$ eV when one of them is Y, and $\Delta G_k = 1.86$ eV when both are Y. (b) Computational flow chart from response function $\chi(t)$ to impedance function $Z(\omega)$. (c) Nyquist plot of the impedance function. The solid line and circles are the result from FDT; crosses are results from the conventional method. The inset shows the equivalent circuit.

is assumed to depend only on the chemical species of the two cations near the diffusing vacancy, as shown in Fig. 1a, and was computed by *ab initio* models [6]. In the conventional approach, the impedance at frequency ω is computed by applying a time-dependent voltage in the x direction, $V(t) = V_0 \sin(\omega t)$. The velocities of N vacancies during the kMC simulation give rise to the "microscopic" current, $I^m(t)$. The "macroscopic" current, $I(t)$, is the ensemble average of $I^m(t)$, and can be computed as an average over many AC cycles after the system has settled into a steady state. After fitting $I(t) = I_0 \sin(\omega t + \phi)$, we obtain the impedance as $Z(\omega) = (V_0/I_0)\, e^{-i\phi}$. This procedure is expensive because it needs to be repeated for every ω of interest.

To develop a more efficient method, it is instructive to consider the YSZ crystal as a linear system whose input is the applied voltage $V(t)$ and output is the response current $I(t)$. The system is described by its response function $\chi(t)$, where $I(t) = \int_{-\infty}^{t} V(t')\chi(t-t')\,dt'$. Let $\hat{\chi}(\omega)$ be the Fourier transform of $\chi(t)$. The impedance function is simply $Z(\omega) = 1/\hat{\chi}(\omega)$. FDT states that the response function $\chi(t)$ to an external stimulus is proportional to the correlation function $C(t)$ of the spontaneous fluctuation in the absence of the stimulus [9]. Applying Kubo's formula [10], we obtain

$$\chi(t) = \begin{cases} C(t)/(k_B T), & t \geqslant 0 \\ 0, & t < 0 \end{cases} \tag{1}$$

where $C(t)$ is the auto-correlation function of microscopic current. It can be computed from kMC simulation data as follows,

$$C(t) = \lim_{\tau\to\infty} \frac{q^2}{\tau L_x^2} \sum_{k\geqslant l} h_k h_l \delta(t + t_k - t_l) \tag{2}$$

where q is the electric charge of vacancy, L_x is the x-length of the supercell, τ is the total time of the simulation, k is summed over all jumps during the simulation, $h_k = (\Delta x)_k$ is the change of the x-coordinate of the jumping vacancy at t_k, and t_k is the time of the jump. By computing $C(t)$ from one kMC simulation in the absence of an applied voltage, we can obtain $Z(\omega)$ of all frequencies by Fourier transform as shown in Fig. 1b.

3. Numerical results and discussion

3.1. Verification of the method

We use this method to calculate the impedance of a $5[100] \times 5[010] \times 5[001]$ supercell of YSZ with 8% dopant concentration at $T = 1800\,K$. Fig. 1c is the Nyquist plot of $Z(\omega) = 1/\hat{\chi}(\omega)$, which is approximately an arc. This behavior can be modelled by the equivalent circuit shown in the inset, consisting of two resistors, R_1 and R_2 and a constant phase element (CPE), i.e.,

$$Z(\omega) = R_1 + \frac{1}{R_2^{-1} + Q(j\omega/\omega_0)^{\alpha}}, \quad j = \sqrt{-1} \tag{3}$$

This equivalent circuit is called the Randles cell [11] and is often used to describe the experimentally measured impedance data. The parameters that best fit the impedance plot in Fig. 1c are: $R_1 = 3.74 \times 10^6\Omega$, $R_2 = 1.34 \times 10^6\Omega$, $\alpha = 0.85$, $Q = 1.35\Omega^{-1}$ and $\omega_0 = 1$ Hz. To verify this result, we also computed the impedance using the conventional method at six different frequencies, $\omega_0 = 0, 20, 40, 80, 100, 200$ GHz. The results are plotted as crosses in Fig. 1c. The excellent agreement between the impedance predicted

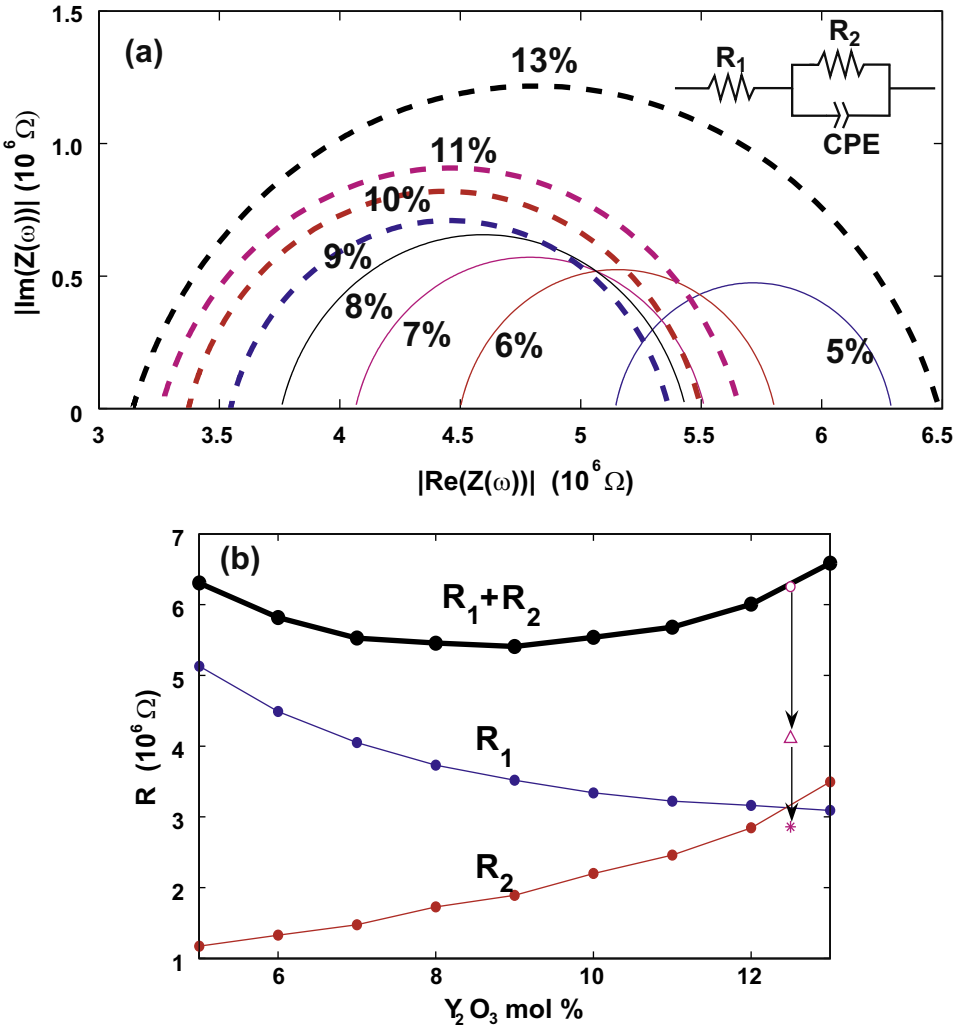

Fig. 2. (a) Nyquist plots for impedance function at different doping concentrations at 1800 K. (b) Parameters for the equivalent circuit as functions of doping concentration. The triangle and the star show the resistance if 50% or 100% of the Y ions form a spherical nano-cluster, respectively.

by the two methods confirms the validity of applying FDT to our kMC simulations of charge transport.

In both methods, the kMC simulations are stopped when the statistical error of the computed impedance becomes smaller than $10^4\ \Omega$. The computational time for the entire frequency range using FDT is only one fifth of the total time to compute the impedance at the six frequencies using the conventional method. Furthermore, a significant advantage of the new method is that it predicts the impedance as a continuous function of frequency. Hence there is no need to decide a priori how many (usually more than 6) frequencies are needed to adequately sample the impedance function. It is interesting to compare our numerical method with the experimental method of electrochemical noise analysis (ENA) [12], which also measures the spontaneous voltage and current fluctuations. But ENA does not use FDT in the form of Kubo's formula, Eq. (1), which is important for our method. So far ENA has only provided information on the modulus $|Z|$, whereas both real and imaginary part of Z are needed to construct the Nyquist plot.

3.2. The effect of doping concentration

The high efficiency of our method allows us to systematically study the effect of doping concentration (from 5% to 13%) on the Nyquist plot, as shown in Fig. 2a. The result at each doping concentration is the average over 40 supercells with different random yttrium distributions. The statistical error in the average over these 40 configurations is about $3 \times 10^4\ \Omega$, which is comparable to the statistical error in the kMC simulation of one configuration ($1 \times 10^4\ \Omega$). Interestingly, from 5% to 9%, the Nyquist plot appears to move to the left as a whole, reducing the impedance both at infinite-frequency (R_1) and zero frequency ($R_1 + R_2$). However, when doping concentration is above 9%, the increase of the arc width R_2 exceeds the decrease of R_1, and the impedance at zero frequency starts to increase. This leads to maximum conductivity ($\propto (R_1 + R_2)^{-1}$) at around 9% doping concentration, which is also observed in experiments and previous simulations.[2]

The existence of a maximum conductivity has been hypothesized to be the result of two competing mechanisms. First, increasing dopant concentration leads to more charge carriers, since every two Y ions create one extrinsic oxygen vacancy. Second, a higher dopant concentration increases the likelihood of having Y ions near the saddle configuration of a diffusion oxygen ion, as shown in Fig. 1a. This increases the energy barrier of diffusion. In the infinite-frequency limit, vacancies do not need to move over long dis-

[2] That the optimum doping concentration of 9% (at $T = 1800$ K) is a higher than the previously reported 8% based on kMC simulations at $T = 600 \sim 1500$ K [7] is consistent with the trend that the optimum doping concentration increases with temperature.

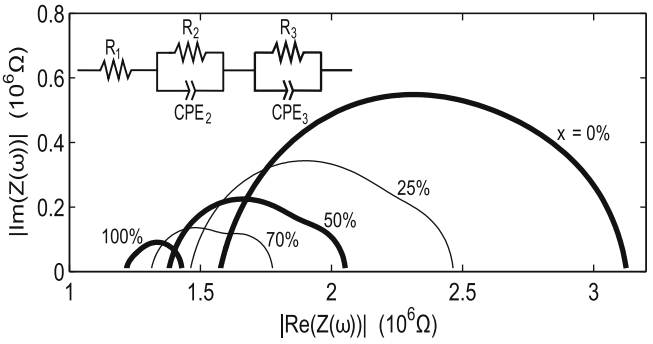

Fig. 3. Nyquist plots for the impedance of YSZ at 12.5% concentration but different Y distributions. A fraction (x) of Y ions are segregated to a spherical nano-cluster while the remaining Y ions are randomly distributed.

tances to contribute to the conductivity. Hence we expect R_1 to be insensitive to the blocking effect of the Y ions, so that the first mechanism is captured by the decrease of R_1 with doping concentration, as shown in Fig. 2b. In the zero frequency limit, the vacancies need to diffuse over long distances to contribute to the conductivity. Hence we expect R_2 to be sensitive to the blocking effect of Y ions, and that the second mechanism is captured by the increase of R_2 with doping concentration, also shown in Fig. 2b. Both R_1 and R_2 can be measured separately by EIS, which would provide an experimental verification of our predictions on their opposite dependence on doping concentration.

3.3. The effect of local microstructure

We now examine the effect of the dopant microstructure on the impedance function when the distribution of Y ions is not completely random. For simplicity, we consider the hypothetical scenario of having a fraction x of Y ions segregate to a spherical cluster, with the remaining Y ions randomly distributed around it. The Nyquist plots for a $10[100] \times 10[010] \times 10[001]$ supercell with 12.5% doping concentration and different cluster sizes, are shown in Fig. 3. Due to the co-existence of two Y distributions (clustered and random), the Nyquist plots deviate from a simple arc and is better described by an equivalent circuit containing an extra pair of resistor and CPE, as shown in the inset of Fig. 3. It is interesting to observe the dramatic change of the Nyquist plot, especially the decrease in the width of the arc $(R_2 + R_3)$ by more than a factor of 7.3, as x increases from 0 to 1. In comparison, the impedance at infinite-frequency (R_1) exhibits a much weaker reduction (by 23%). This confirms our earlier hypothesis that the width of the arc in the Nyquist plot is a good measure of the interaction between Y ions and the oxygen vacancies, i.e. the second mechanism controlling the ionic conductivity. Specifically, for larger x, there are more pathways for a diffusing vacancy to traverse the entire supercell without encountering any Y ions in its path.

Fig. 3 shows that the distribution of Y ions have a dramatic effect on conductivity. The 34% reduction of impedance as x goes from 0 to 50% is more significant than what can be produced by changing the concentration from 12.5% to 9% while keeping the random distribution, as shown in Fig. 2. This suggests that if we could engineer the microstructure of dopants by promoting nano-scale segregation, the ionic conductivity would be greatly enhanced. With the advent of modern fabrication techniques, such as molecular beam epitaxy (MBE) and atomic layer deposition (ALD) [13–15], the realization of such metastable, segregated nanostructures appears possible. The general idea of improving ionic conductivity by engineering desirable nanostructures has shown promise in $BaF_2 : CaF_2$ multi-layers [16,17], although the effect was attributed to space charge effects instead of the blocking effect of dopant cations proposed here.

4. Conclusion

We have shown that the fluctuation–dissipation theorem can be used to compute electrical impedance of all frequencies from a single equilibrium kMC simulations. Our method can be easily generalized to model systems with surfaces and grain boundaries [2], as well as local impedance imaging experiments using an AFM probe [18].

Acknowledgement

This work is partly supported by the DOE/SciDAC project on Quantum Simulations of Materials and Nanostructures. Eunseok Lee acknowledges support from the Samsung Scholarship Foundation.

References

[1] R. O'Hayre, S.-W. Cha, W. Colella, F.B. Prinz, Fuel Cell Fundamentals, Wiley, New York, 2006 (Chapter 7).
[2] S. Hui, J. Roller, S. Yick, X. Zhang, C. Decés-Petit, Y. Xie, R. Maric, D. Ghosh, J. Power Sources 172 (2007) 493.
[3] A. Bard, L. Faulkner, Electrochemical Methods: Fundamentals and Applications, second ed., Wiley, 2001.
[4] Y. Yamamura, S. Kawasaki, H. Sakai, Solid State Ionics 126 (1999) 181.
[5] R. Morgado, F.A. Oliveira, G.G. Batrouni, A. Hansen, Phys. Rev. Lett. 89 (2002) 100601.
[6] R. Krishnamurthy, Y.-G. Yoon, D.J. Srolovitz, R. Car, J. Am. Ceram. Soc. 87 (2004) 1821.
[7] R. Pornprasertsuk, P. Ramanarayanan, C.B. Musgrave, F.B. Prinz, J. Appl. Phys. 98 (2005) 103513.
[8] J. Fergus, J. Power Sources 162 (2006) 30.
[9] D. Chandler, Introduction to Modern Statistical Mechanics, Oxford University Press, 1987, p. 237.
[10] R. Kubo, Rep. Prog. Phys. 29 (1966) 255.
[11] N. Fouquet, J. Power Sources 159 (2006) 905.
[12] F. Mansfeld, Z. Sun, C.H. Hsu, Electrochim. Acta 46 (2001) 3651.
[13] Y.R. Li, Z. Liang, Y. Zhang, J. Zhu, S.W. Jiang, X.H. Wei, Thin Solid Films 489 (2005) 245–250.
[14] C.-h. Chiu, Z. Huang, C.T. Poh, Phys. Rev. Lett. 93 (2004) 136105.
[15] C. Bae, H. Shin, J. Moon, M.M. Sung, Chem. Mater. 18 (2006) 1085–1088.
[16] N. Sata, K. Eberman, K. Eberl, J. Maier, Nature 408 (2000) 946.
[17] S. Adams, E.S. Tan, Solid State Ionics 179 (2008) 33.
[18] R. O'Hayre, M. Lee, F.B. Prinz, J. Appl. Phys. 95 (2004) 8382.